Hindawi
Advances in Materials Science and Engineering
Volume 2021, Article ID 7185616, 13 pages
https://doi.org/10.1155/2021/7185616

Research Article

Experimental and Numerical Analyses of the Thermal Regime of a Traditional Embankment in Permafrost Regions

Qihang Mei,[1,2] **Ji Chen**,[1,2] **Shouhong Zhang**,[3] **Xin Hou**,[1,2] **Jingyi Zhao**,[1,2] **Jinchang Wang**,[3] **Haiming Dang**,[3] **Guojun Liu**,[1] **and Guilong Wu**[1]

[1]*Beiluhe Observation and Research Station of Frozen Soil Engineering and Environment, State Key Laboratory of Frozen Soil Engineering, Northwest Institute of Eco-Environmental and Resources, Chinese Academy of Sciences, Lanzhou 730000, China*
[2]*University of Chinese Academy of Sciences, Beijing 100049, China*
[3]*China Railway Qinghai-Tibet Group Co., Ltd., Xining 810007, China*

Correspondence should be addressed to Ji Chen; chenji@lzb.ac.cn

Received 6 May 2021; Accepted 30 June 2021; Published 23 July 2021

Academic Editor: Xiangtian Xu

Traditional embankment is widely used in the permafrost regions along the Qinghai-Tibet Railway (QTR) because of its simple construction and lower cost. However, this form of embankment has insufficient ability to resist external thermal disturbance. To clarify the thermal characteristics of traditional embankment under climate warming, the ground temperature change process of section K1068 + 750 of the QTR was analysed in this study. Based on the field monitoring data from 2006 to 2019 and the established heat transfer model, the past and future changes of permafrost thermal regime under the embankment were analysed. The results show that the degradation of permafrost under the embankment is faster than that under the undisturbed site due to the combined of embankment construction and climate warming. The sunny-shady slope effect related to embankment orientation makes the distribution of permafrost temperature under embankment asymmetric. In the long term, permafrost degrades both under the undisturbed site and embankment. The continuous degradation of permafrost causes the settlement and deformation of embankment, especially the asymmetric degradation of permafrost on sunny side and shady side will cause longitudinal cracks on the embankment. Therefore, timely application of strengthening measures which can slow down the degradation of permafrost and adjust the uneven ground temperature on the sunny and shady sides under the embankment is of great significance to the safety of the traditional embankment.

1. Introduction

The Golmud-Lhasa section of the Qinghai-Tibet Railway (QTR) with a length of 1142 km was completed and started operation in 2006 [1]. It covers 550 km of continuous permafrost regions, 50% of which belong to warm permafrost areas with the mean annual ground temperature (MAGT) higher than −1°C [2]. The high thermal sensitivity of warm permafrost makes the stability of embankment in these areas significantly affected by changes in the external environment temperature [3]. Many studies based on field monitoring have shown that with the climate warming and the change of land-surface energy balance caused by the construction of embankment, the permafrost along the QTR has been extensively degraded, especially under the traditional embankment [4–7]. The degradation of permafrost has caused the settlement deformation of the embankment, which reduces the smoothness of the railway track and poses a threat to the safe operation of the train [8–11]. In addition, in the section of the QTR that is not in the north-south direction, there is a sunny and shady slope effect caused by different heat absorption on both sides of embankment that makes the ground temperature under two sides of the embankment slope different [12]. The asymmetry of the permafrost temperature distribution on the sunny and shady sides of the embankment causes asymmetrical settlement

and eventually forms longitudinal cracks which may make the embankment fail [13, 14]. Considering the above problems faced by the embankment of the QTR under climate warming, it is necessary to timely evaluate the stability of the embankment that may be unstable.

The study on the embankment stability of the QTR is mainly carried out through field monitoring and numerical simulation. Most of the monitoring data of ground temperature and deformation of the embankment come from the long-term monitoring program of the QTR which started to work in October 2005. Based on ground temperature and deformation data, the researchers analysed the thermal response of permafrost under the embankment to climate and human activity [15–17]. Furthermore, by comparing the thermal stability and deformation stability of different embankment forms, the cooling ability of each structure is evaluated [5, 18–20]. However, due to the limitations of field conditions and the lack of enough monitoring data, methods such as numerical simulations other than field monitoring have also been used to study the embankment stability in permafrost regions. For example, for some new forms of embankment, the stability can be determined by establishing a suitable mathematical model before the embankment construction [21–24]. The numerical simulation can also be used to analyse the degradation progress of permafrost under the embankment and the embankment deformation in the future under climate change, so as to find the embankment that needs to be strengthened in time [25–27]. The simultaneous use of field monitoring and numerical simulation in the study not only helps to solve more engineering problems, but also improves the accuracy of the conclusions.

In this paper, the change process of ground temperature is analysed based on the ground temperature monitoring data of section K1068 + 750 from 2006 to 2019. In addition, a heat transfer model is established to predict the change of thermal regime of the section in the next few decades. The research includes the degradation characteristics of permafrost under the embankment and the difference of permafrost temperature distribution on both sides of the embankment caused by the sunny-shady slope effect. The analysis results can be used as the basis for the selection of strengthening measures for this section and provide reference for the stability evaluation of similar projects in the future.

2. Field Observations

2.1. Site Description. The study section, with the mileage of K1068 + 750 along the QTR, is located in the Chumaer River High Plain (Figure 1). The monitoring results of adjacent meteorological stations show that the mean annual air temperature in this region is −2.9°C [28]. As shown in Figure 2, the air temperature from 2007 to 2016 close to the ground shows that the temperature is between −28.9°C and 13.4°C, and it is higher than 0°C from June to September every year. The altitude of the study area is 4552 m, and the vegetation coverage is about between 30% and 50%. A borehole survey conducted in 2004 shows that the MAGT and the permafrost table (PT) under the study section is −0.5°C and 5 m, respectively, at undisturbed ground. In this paper, the PT is calculated by linear interpolation of adjacent depths of 0°C isotherm. The results of this survey also show that the permafrost in this region is mainly ice-rich permafrost (volume ice content less than 10% to 20%) and icy permafrost (volume ice content is between 10% and 20%). The embankment was built in the warm season of 2002 with a height of 2.8 m. This embankment is a traditional earthen embankment without any proactive cooling measures. The embankment orientation is 241.6°, which means that the intensity of the solar radiation on both sides of the slopes is different.

2.2. Ground Temperature Monitoring. In order to monitor the thermal stability of the embankment, a ground temperature monitoring system was built in this section and started operation at the end of 2005 as shown in Figure 3. The monitoring system consists of an undisturbed site monitoring borehole and two embankment monitoring boreholes. Since it is 20 m away from the slope toe of the embankment, it can be considered that the ground temperature of the undisturbed site monitoring borehole with a depth of 16 m is not affected by the embankment. Two embankment monitoring boreholes with a depth of 20 m are located on both sides of the embankment, which are used to monitor the temperature of the embankment and the soil on the sunny side and the shady side, respectively. In these boreholes, temperature sensors are distributed every 0.5 m from 0 m to 10 m depth and every 1 m below 10 m depth. These temperature sensors are made by the State Key Laboratory of Frozen Soil Engineering with an accuracy of ±0.05°C. The ground temperature data is automatically collected by the data logger (DT500) once a day. In the analysis of this paper, the ground temperature used is the monthly mean value obtained by averaging daily data.

2.3. Observational Results. Figure 4 shows the change process of ground temperature on the sunny side and shady side of the embankment from 2006 to 2019. It is found that there are differences in their thermal regimes between the two sides. First, since 2006, the ground temperature on the sunny side has been higher than that on the shady side at the same depth. The most representative one is the depth of PT on the sunny side that is more than 5 m, which is deeper than that on the shady side. Second, the depth variation of different isotherms indicates that the temperature variation rate of permafrost on both sides of the embankment is different. In Figure 4(a), the −0.1°C isotherm declined from 7.67 m in 2006 to 10.13 m in 2019, with a decrease of 2.46 m. And in Figure 4(b), the −0.2°C isotherm has increased from 6.75 m in 2006 to 6.40 m in 2019, which is only a change of 0.35 m. In addition, the 0°C isotherm on the sunny side declined from 7.69 m in 2006 to 9.18 m in 2019, while the 0°C isotherm on the shady side rose from 5.03 m in 2006 to 4.48 m in 2019. The change of 0°C isotherm indicates that the depth of the PT on the sunny side increases by 1.49 m while the depth of the PT on the shady side decreases by 0.55 m. The

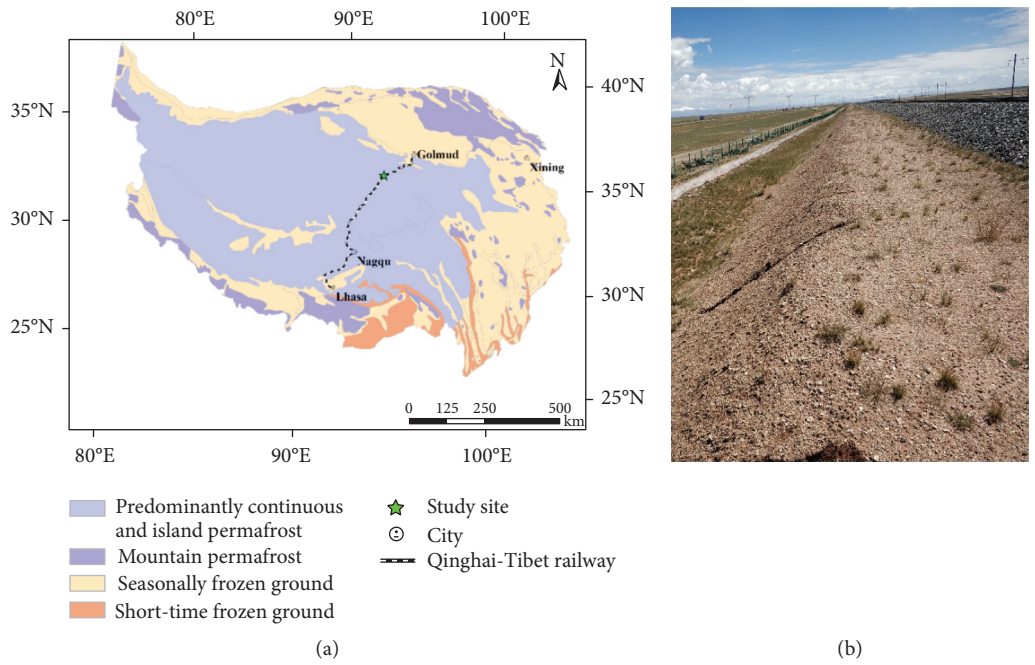

Figure 1: Location (a) and image (b) at section K1068 + 750.

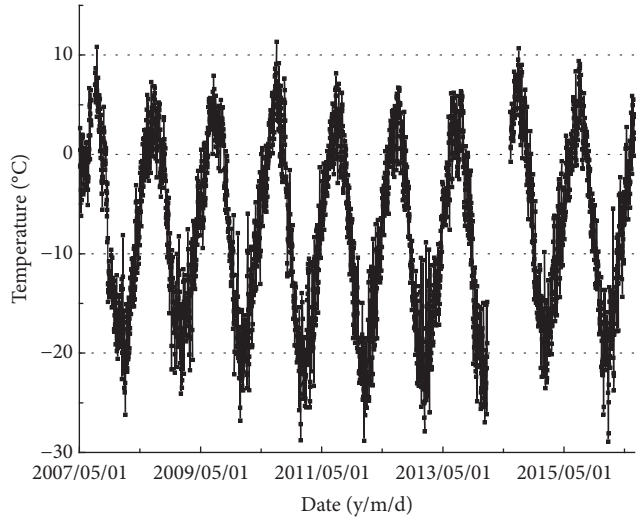

Figure 2: Air temperature changers of section K1068 + 750.

change of the above isotherms shows that the ground temperature in the shallow permafrost (with a depth of less than 10 m) on the sunny side increases significantly, while it decreases slightly on the shady side.

Figure 5 shows the ground temperature at different depths when the annual maximum melting depth occurs from 2006 to 2019, with an interval of three years. Affected by the drastically changing external environment temperature, the ground temperature in the active layer has no obvious regularity. The permafrost layers on the sunny and shady sides of the embankment showed different changes from 2006 to 2018. On the sunny side of the embankment, the permafrost is in the process of warming in both the shallow and deep layers (with a depth of greater than 10 m), and the warming range is between 0.05°C and 0.22°C (Figure 5(a)). Although the warming range decreases with the increase of depth, the temperature of permafrost above 18 m is warming up significantly, all of which are greater than 0.1°C. On the shady side of the embankment, the upper permafrost temperature decreases while the lower permafrost temperature increases (defined the upper and lower parts with a depth of 7 m) (Figure 5(b)). Both the increase and decrease of ground temperature are not greater than 0.1°C, which means that the thermal regime of permafrost is stable on the shady side of the embankment.

To further investigate the embankment thermal regime variation characteristics and the difference of ground temperature between the sunny and shady sides, the ground

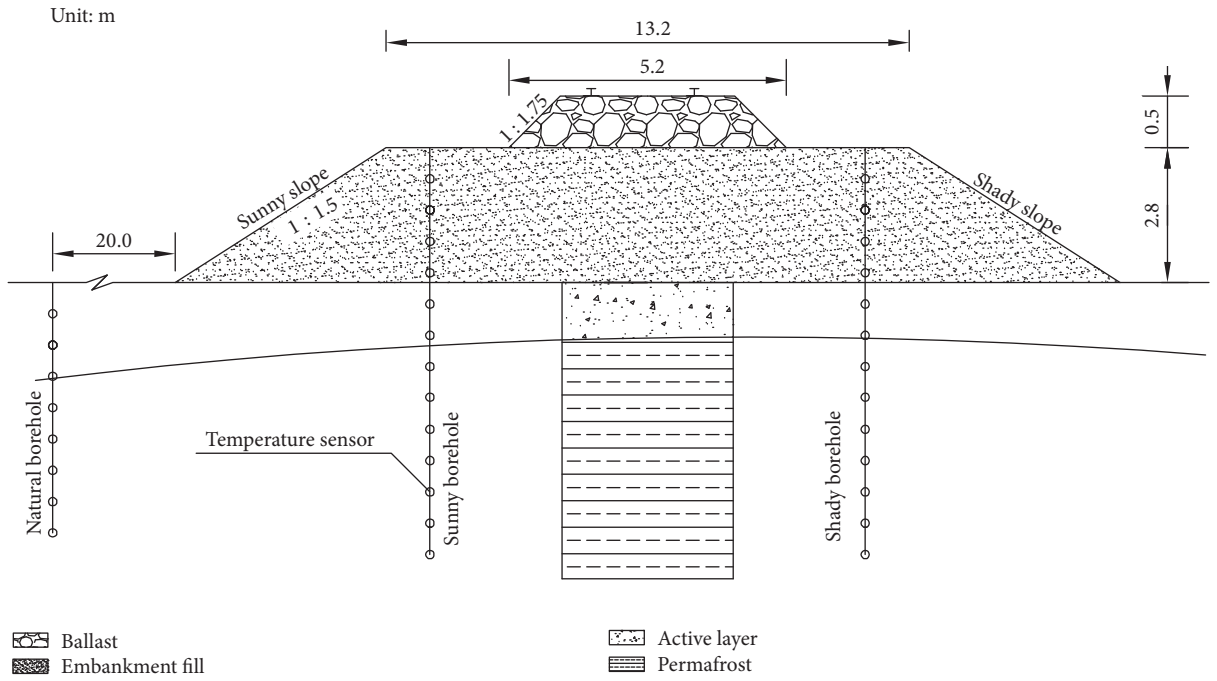

Figure 3: Monitoring system for the ground temperature at section K1068 + 750.

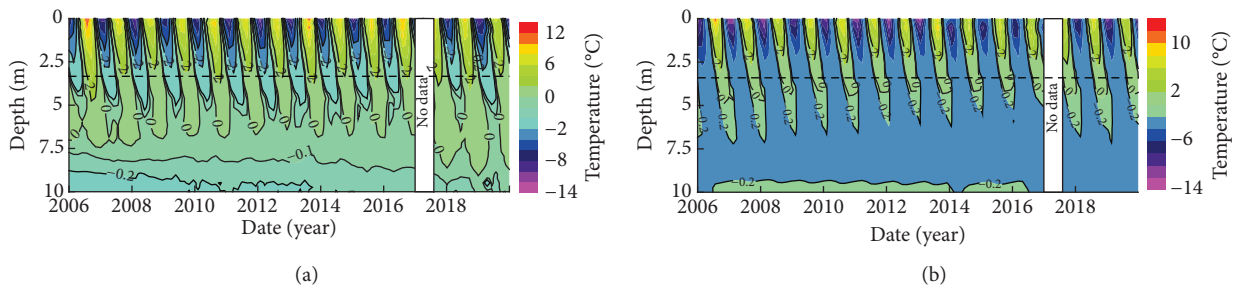

Figure 4: Ground temperature isotherms at the sunny shoulder (a) and the shady shoulder (b). The dotted line in the figure represents the original natural surface.

temperature of permafrost at depths of 8 m and 12 m was analysed, respectively, as shown in Figure 6. In 2006, there was permafrost at 8 m depth on the sunny and shady sides, and the ground temperature is −0.13°C and −0.25°C, respectively (Figure 6(a)). After 2006, the ground temperature on the sunny side has gradually increased and reached above 0°C in 2017, which means that the soil here has been degraded to seasonal permafrost. The mean annual temperature at 8 m depth on the sunny side increased from −0.12°C in 2006 to 0.01°C in 2019, with an increase of 0.13°C. However, the ground temperature at 8 m depth on the shady side changes in stages. In the first stage, the mean annual temperature decreased from −0.36°C in 2006 to −0.42°C in 2014. Then, in the second stage, the mean annual temperature increased from −0.42°C in 2014 to −0.3°C in 2019. From 2006 to 2019, the change of ground temperature on the sunny side is only 0.06°C, which is twice less than that on the sunny side. The variation trend of ground temperature at 12 m depth on the sunny side is similar to that at 8 m, which is continuously increasing (Figure 6(b)). The mean annual temperature on the sunny side increased from −0.37°C in 2006 to −0.22°C in 2019, increased by 0.15°C. The ground temperature on the shady side is basically stable, increased by 0.06°C from 2006 to 2019. The above analysis shows that from 2006 to 2019, the permafrost on the sunny side has undergone significant degradation, while the permafrost on the shady side is relatively stable.

3. Numerical Simulations

Obtaining long-term ground temperature data is conducive to further analyse the thermal performance of embankment in permafrost regions. Therefore, based on the reasonable simplification of K1068 + 750 embankment section of the QTR, a heat transfer model is established to investigate the thermal regime of the embankment under climate warming.

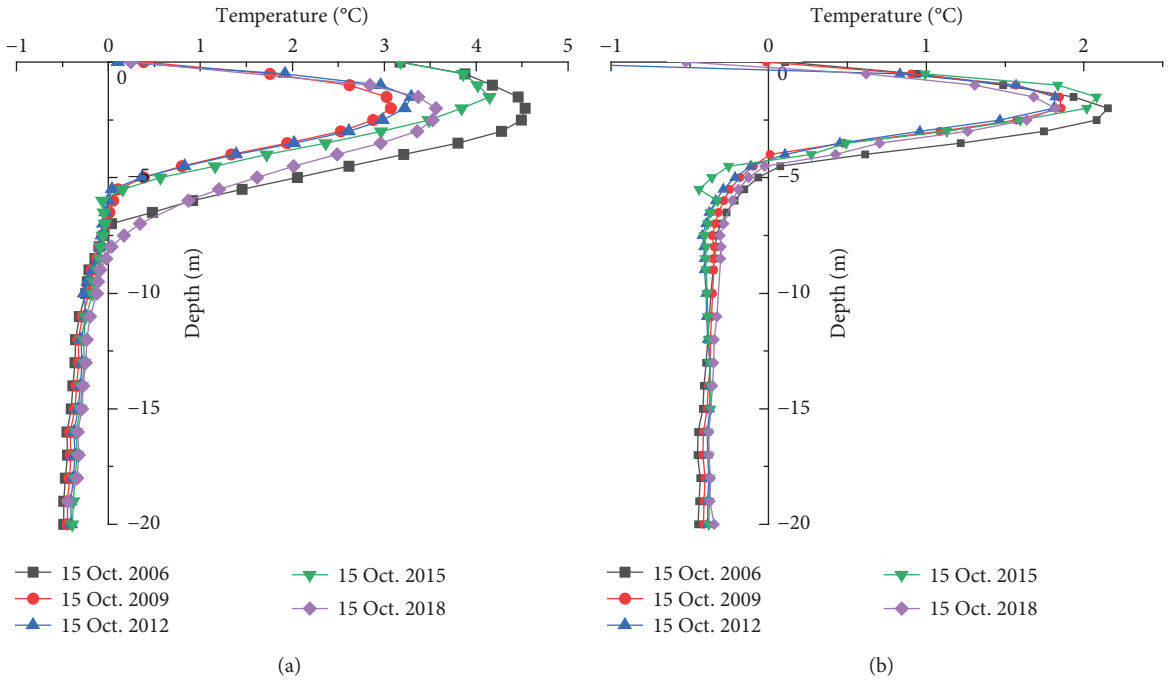

Figure 5: Ground temperature profiles on Oct. 15th at the sunny shoulder (a) and the shady shoulder (b) in different years.

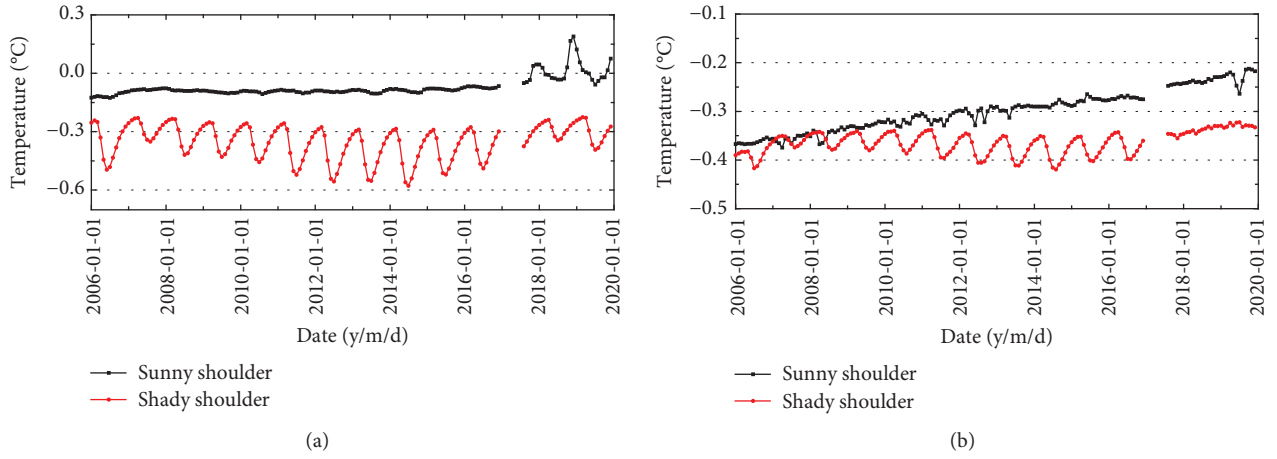

Figure 6: Variation of ground temperature at 8 m (a) and 12 m (b) on the sunny and shady sides of embankment.

3.1. Governing Equations. Previous study has shown heat transport by convective heat transfer was only 1/100 to 1/1000 of that by heat conduction in soil [29]. Therefore, in the heat transfer calculation, only the heat conduction of soil and latent heat of ice-water phase change are considered, and convection heat transfer is ignored. The governing equation of heat transfer calculation in embankment and soil layer is as follows [30, 31]:

$$C^e\frac{\partial T}{\partial t} = \frac{\partial}{\partial x}\left(\lambda^e\frac{\partial T}{\partial x}\right) + \frac{\partial}{\partial y}\left(\lambda^e\frac{\partial T}{\partial y}\right), \quad (1)$$

where C^e is the effective volumetric heat capacity of soil, λ^e is the thermal conductivity of soil, T is the temperature, and t is the time.

It is assumed that the heat capacity and thermal conductivity of the materials do not change with temperature outside the temperature range $T_m \pm \Delta T$ where the phase transition occurs. And within the temperature range of phase transition, the latent heat of phase transition of the water-bearing materials is simulated by the method of sensible heat capacity, as shown in the following equations [32]:

$$C^e = \begin{cases} C_f, & T < (T_m - \Delta T), \\ \dfrac{L}{2\Delta T} + \dfrac{C_f + C_u}{2}, & (T_m - \Delta T) < T < (T_m + \Delta T), \\ C_u, & (T_m + \Delta T) < T, \end{cases} \tag{2}$$

$$\lambda^e = \begin{cases} \lambda_f, & T < (T_m - \Delta T), \\ \lambda_f + \dfrac{\lambda_u - \lambda_f}{2\Delta T}\left[T - (T_m - \Delta T)\right], & (T_m - \Delta T) < T < (T_m + \Delta T), \\ \lambda_u, & (T_m + \Delta T) < T, \end{cases} \tag{3}$$

where C_f and C_u are the volumetric heat capacities of the materials in the frozen and the melting states, respectively; λ_f and λ_u are the thermal conductivity of the materials in the frozen and the melting states, respectively. L is the latent heat per unit volume. The influence of soil pores and solutes may make the freezing temperature below 0 °C, which means that the values of T_m and ΔT need to be determined in different situations. In this study, the values of T_m and ΔT in the calculation were 0°C and 0.5°C, respectively.

3.2. Physical Model. The physical model of the embankment is shown in Figure 7. Considering that the soil layer is considered to be infinite in the longitudinal direction and no heat transfer occurs, the 2D heat transfer model is established in this study [23]. Above the natural surface, the embankment can be divided into two parts: embankment fill and ballast. Referring to the field measurement, the heights of the two parts in the model are 2.8 m and 0.5 m, respectively. Based on the thermal disturbance range of embankment, the depth and horizontal width of the part under the embankment in the model are set as 30 m and 80 m, respectively. The borehole data show that there is sandy soil (0–3 m), gravel soil (3–13 m), and strongly weathered stone (13–30 m) under the natural surface. According to the existing experimental results and geological data, the thermal parameters of different materials in this model are determined as shown in Table 1 [23, 33].

3.3. Boundary and Initial Conditions. The upper thermal boundary of the model is affected by various factors such as external environmental temperature and solar radiation. The difference in thermal characteristics can divide the upper boundary conditions of the model into natural ground surface (AB and IJ), sunny slope surface (BCDE), shady slope surface (FGHI), and top surface of embankment (EF). The simplified ground temperature change process at the upper boundary can be described as follows [34]:

$$T = T_0 + A\sin\left(\frac{2\pi t}{8760} + \varphi\right) + R_0 t, \tag{4}$$

where T is the boundary surface temperature; T_0 is the mean annual temperature of the boundary surface; A is the annual amplitude temperature of the boundary surface; φ is the initial phase angle, which is $\pi/2$ in this model; R_0 is the rate of climate warming; and R_0 in this model is taken as 0.052°C/8760 h according to the conclusion of the temperature increase of 2.6°C in the next 50 years studied by Qin et al. [35]. Based on the adherent layer theory, the values of T_0 and A are determined by analysing field monitoring data and referring to previous studies as shown in Table 2 [13, 36].

This model also includes the wall boundaries on the left and right sides (AL and JK) that are considered adiabatic and the bottom boundary (LK) with a heat flow of 0.06 W/m^2 [37].

Assuming that no embankment is built above the natural ground surface and the climate warming rate R_0 is 0, equation (4) is used as the upper boundary condition to calculate for 50 years until the ground temperature distribution is stable. The calculated result is taken as the initial temperature field under the natural ground surface, and the initial temperature inside the embankment is assumed to be 10°C.

In the first few years after the construction, the internal temperature field of embankment is significantly affected by the construction. Therefore, the starting time of this simulation is determined to be July 2006, when the embankment construction had been completed for 4 years and the internal temperature was basically stable.

3.4. Model Validation. With the above settings, the model is used to simulate the change process of the ground temperature distribution at section K1068 + 750 in the next 50 years. In order to validate the accuracy of the model, ground temperatures of the section on the sunny and shady sides in July 2012 and January 2013 when the surface ground temperature was the highest and the lowest were selected and compared, as shown in Figure 8. The complex environmental factors and simplification of boundary conditions make the simulated ground temperature and measured value have errors in the active layer, which is most significant on the sunny side in July 2012 (Figure 8(a)). As shown in Figures 8(a)–8(d), the simulated values of the ground temperature in the permafrost layer on both sides of the

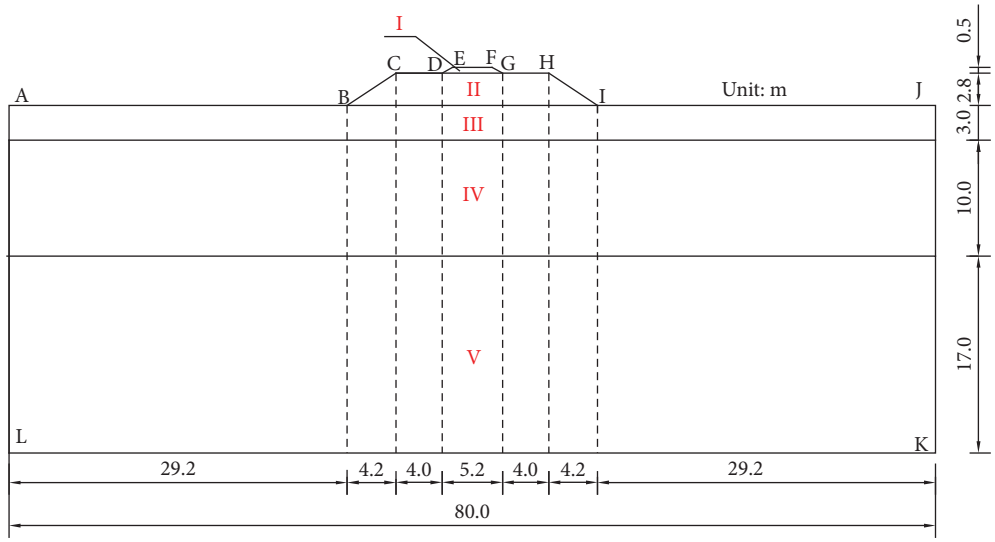

Figure 7: Physical model profile of section K1068 + 750. I: ballast; II: embankment fill; III: sandy soil; IV: gravel soil; V: strongly weathered stone.

Table 1: Thermal parameters of different materials in the model.

Properties	ρ (kg·m^{-3})	C_f (J·m^{-3}·°C^{-1})	C_u (J·m^{-3}·°C^{-1})	λ_f (W·m^{-1}·°C^{-1})	λ_u (W·m^{-1}·°C^{-1})	L (J·m^{-3})
Ballast	2100	1.006×10^6	1.006×10^6	0.346	0.346	0
Embankment fill	1980	3.781×10^6	4.415×10^6	1.98	1.91	2.04×10^7
Sandy soil	1900	2.329×10^6	2.561×10^6	2.61	1.92	2.26×10^7
Gravel soil	1400	1.434×10^6	1.756×10^6	1.63	0.93	2.30×10^7
Strongly weathered stone	1700	3.138×10^6	3.568×10^6	1.82	1.47	3.81×10^7

Note. ρ is the density of the material; L is the latent heat per unit volume.

Table 2: Temperature parameters of upper boundary condition.

Variables	T_0 (°C)	A (°C)
Natural ground surface	−0.5	10
Sunny slope surface	1	12
Shady slope surface	−1.2	13
Top surface of embankment	0.38	14.5

embankment agree with the measured values, which indicates that the model can be used to simulate the changes of the permafrost under section K1068 + 750.

3.5. Numerical Results. Figure 9 shows the ground temperature distribution of embankment at different times calculated by the model. Based on the analysis of the ground temperature distribution under the embankment in 2022, which is 20 years after the embankment construction, it is found that the ground temperature under the embankment is significantly higher than that at the same depth of undisturbed site (Figure 9(a)). For example, there is an unfrozen zone surrounded by 0°C isotherm under the embankment, while the undisturbed site soil at the same depth is frozen. In addition, the depth of the −0.4°C and −0.5°C isotherms under the embankment in the figure is greater than that of the undisturbed sites on both sides, which also indicates that the ground temperature under the embankment is higher. It can also be found in Figure 9(a) that the ground temperature on the sunny side of the embankment is higher than that on the shady side. An obvious feature is that the unfrozen zone surrounded by the 0°C isotherm under the embankment mentioned above is closer to the sunny slope. And the −0.4°C and −0.5°C isotherms are also deeper on the sunny side.

Comparing Figures 9(a)–9(f) (corresponding to the 20th, 25th, 30th, 35th, 40th, and 50th year after the embankment construction, respectively) showed that the ground temperature under both the undisturbed site and the embankment increased year by year. The 0°C isotherm of the undisturbed site declined from 5.47 m in 2022 to 10.50 m in 2052, with a decrease range of 5.03 m (the depth is calculated from the top surface of the embankment). The 0°C isotherm under the center of the embankment has declined from 2.51 m in 2022 to 12.95 m in 2052, with a decreasing range of 10.44 m. Similarly, the isotherms of −0.2°C, −0.4°C, and −0.5°C decrease greatly. The change of the above isotherms

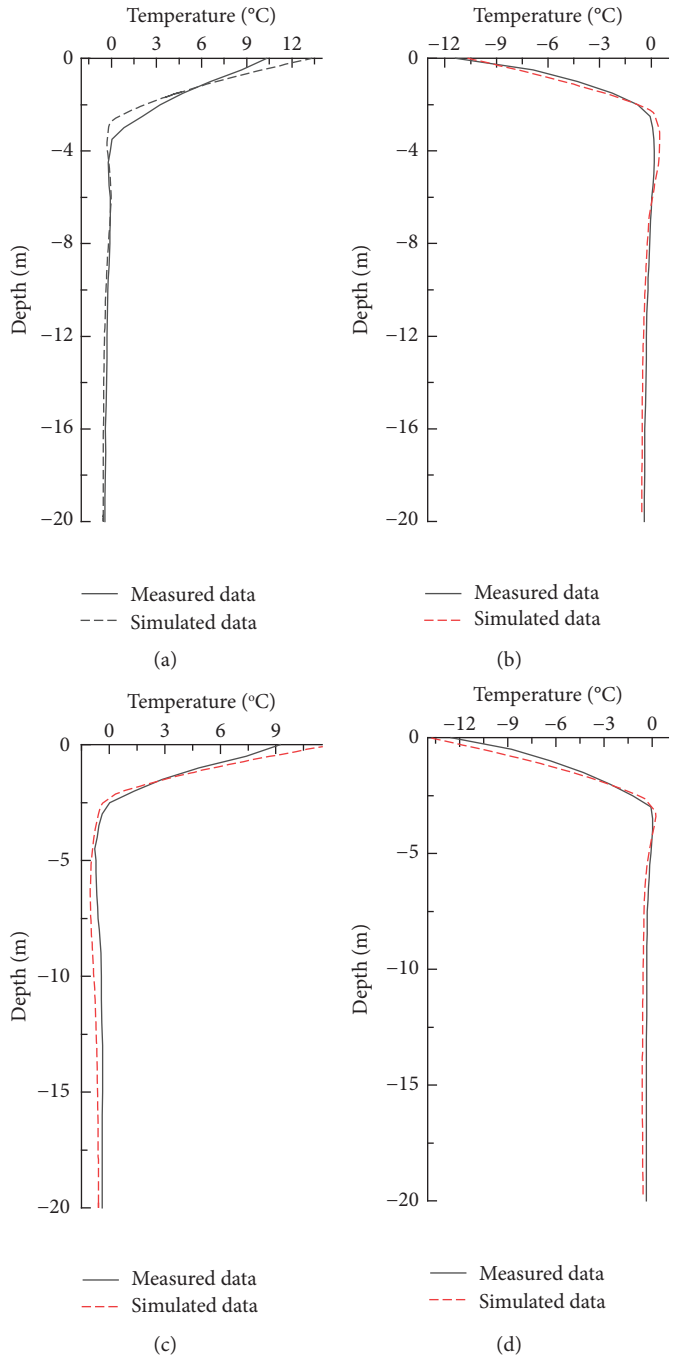

Figure 8: Simulated and measured temperature values at different depths on the sunny and shady slope. (a) Sunny shoulder Jul. 2012. (b) Sunny shoulder Jan. 2013. (c) Shady shoulder Jul. 2012. (d) Shady shoulder Jan. 2013.

in Figure 9 also indicates that the increase of ground temperature under the embankment is greater than that of the undisturbed site from 2022 to 2052.

To explore the process of permafrost warming under the embankment and the difference of ground temperature between the sunny and shady sides in more details, the simulated changes of ground temperature at different depths were analysed from 2020 to 2050, as shown in Figure 10. The temperature profile on October 15 was selected for analysis because it reached the annual maximum melting and the permafrost under the embankment had the worst thermal stability. On the sunny side of the embankment, the PT declined from 6.52 m in 2020 to 12.61 m in 2050, with a decline range of 6.09 m (Figure 10(a)). The permafrost beneath the embankment continued warming from 2020 to 2050. And the same as the monitoring results of ground temperature from 2006 to 2019, the warming range decreases with the increase of depth. The ground temperature near the original permafrost table (at 7 m depth) increased by 1.41°C. At the depth of 15 m, the ground temperature

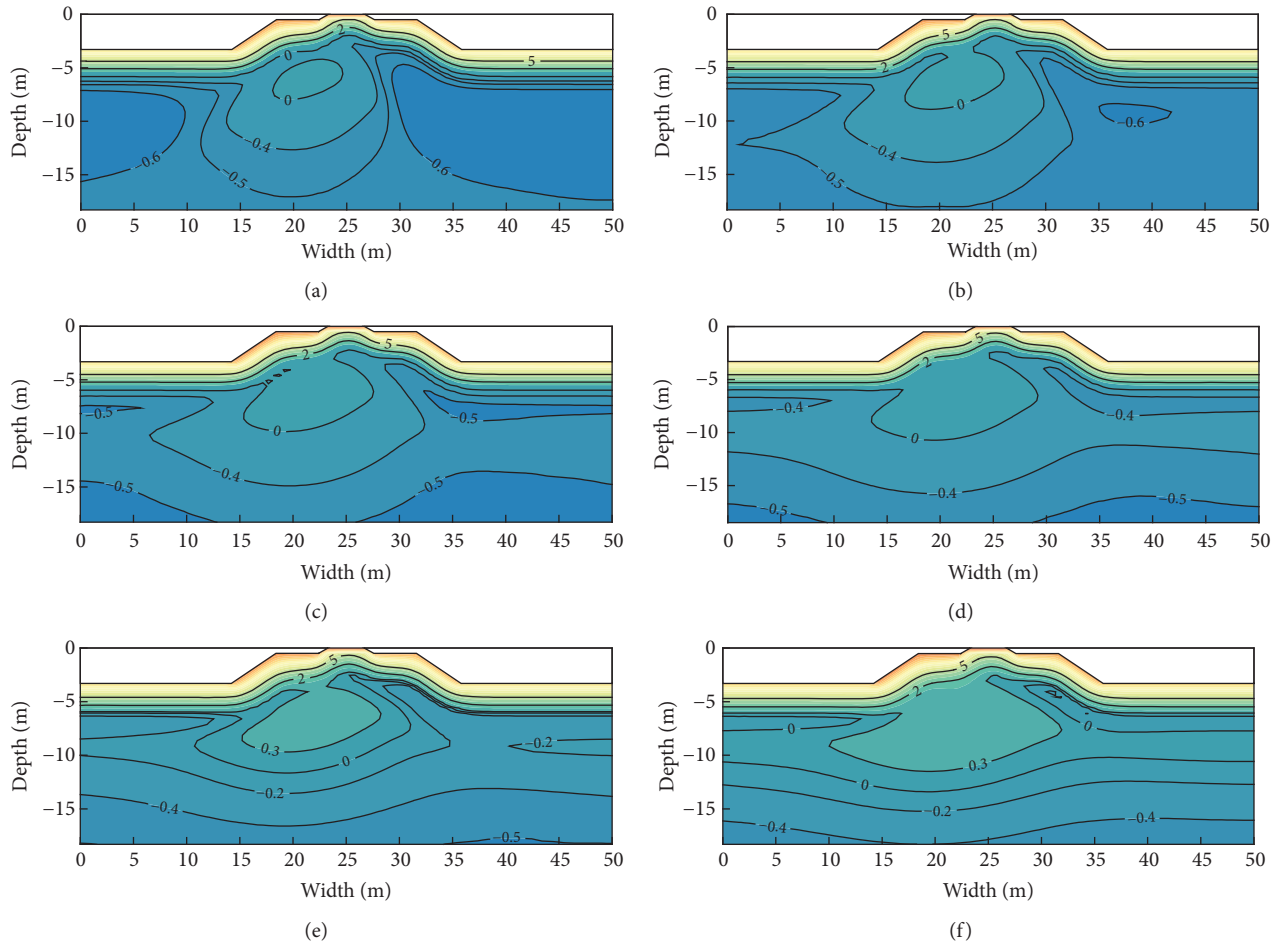

Figure 9: Simulated ground temperature distribution of embankment (unit: ˚C). (a) 2022/7/1. (b) 2027/7/1. (c) 2032/7/1. (d) 2042/7/1. (e) 2037/7/1. (f) 2052/7/1.

increased by 0.24˚C from 2020 to 2050. The analysis of ground temperature change on the shady side of embankment shows that the PT declined from 4.05 m in 2020 to 10.24 m in 2050, with a decline range of 6.19 m (Figure 10(b)). The permafrost on the shady side is also warming and the range of warming decreases with increasing depth. At a depth of 7 m, the ground temperature increased by 0.82˚C, which was significantly less than that at the sunny side. At a depth of 15 m, the ground temperature on the shady side increased by 0.21˚C, which is smaller than that on the sunny side. Changes in permafrost thickness (corresponding to changes in the PT) and temperature both indicate that permafrost degradation is faster on the sunny side.

It is worth noting that there is an obvious difference between the simulated depth of the PT 6.52 m in 2020 and the measured depth of the PT 9.18 m in 2019. The reason for this phenomenon is that the PT is significantly affected by the active layer above it, which fluctuates greatly in temperature. However, as has been verified above, this phenomenon mainly occurs in the shallow layer, and the results obtained by the simulation are generally reliable.

4. Discussion

Both human activities and environmental changes can affect the thermal state of permafrost and cause permafrost degradation. The degradation of permafrost in the undisturbed site is mainly caused by the continuous warming of the climate, while the degradation of permafrost under the embankment is affected by both engineering activities and climate warming. The influence of climate warming on permafrost is mainly determined by geological conditions and surface factors such as vegetation conditions [38]. The engineering activity of embankment construction not only changes the original natural surface, but also affects the water-heat balance of soil [39–41]. Therefore, the degradation rate of permafrost under embankment is generally much faster than that of permafrost in the adjacent undisturbed site [42]. This conclusion has also been verified in

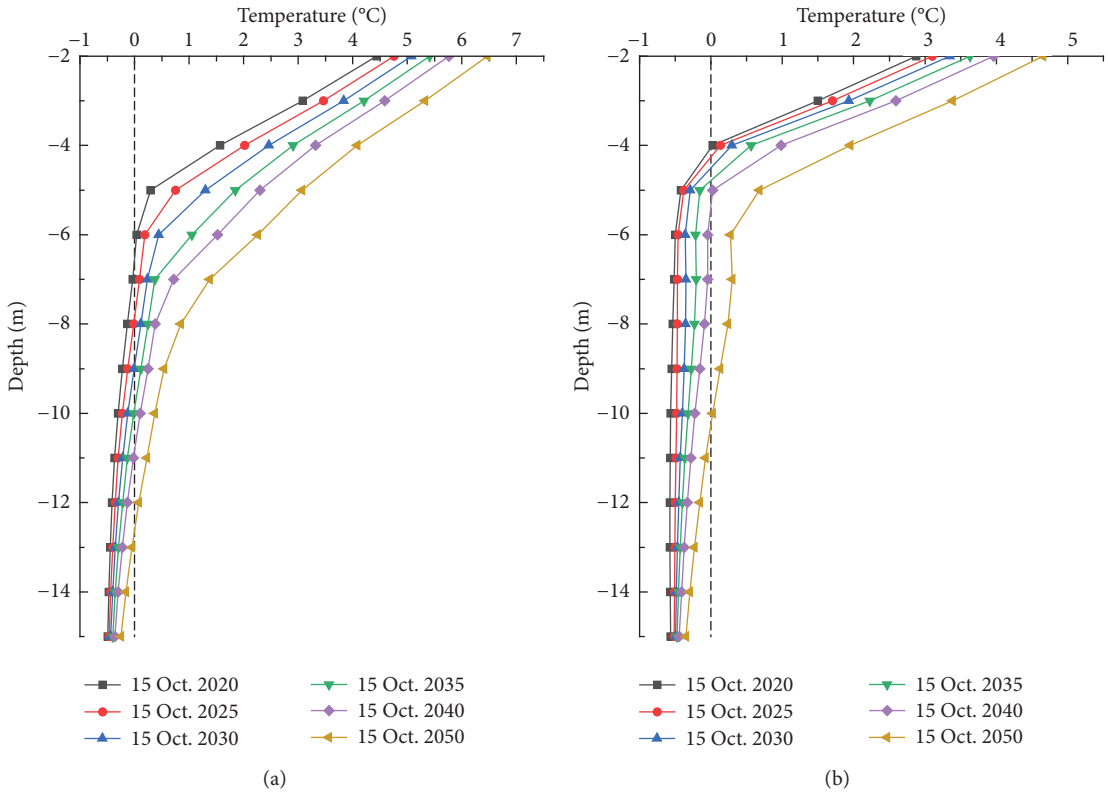

Figure 10: Simulated ground temperature profiles on Oct. 15th at the sunny shoulder (a) and the shady shoulder (b).

the simulation results of this study. For example, from 2022 to 2052, the decreasing depth of 0°C isotherm in the center of embankment is twice that of the undisturbed site, as shown in Figure 8. The monitoring and simulation results show that the permafrost degradation occurs in the undisturbed site and the embankment at section K1068 + 750 at different rates.

The difference of solar radiation on both sides of the subgrade determined by the direction of the embankment results in the uneven degradation of permafrost under permafrost [43–45]. The study shows that in the northern hemisphere, the temperature difference in the embankment with east-west orientation is the largest, and that with south-north orientation is the smallest, while K1068 + 750 is close to northeast-southwest orientation [46, 47]. Therefore, on section K1068 + 750, although the embankment is geometrically symmetric, the distribution of ground temperature on the sunny side and the shady side is different. From 2006 to 2019, the permafrost under the sunny side of the embankment has degraded significantly, characterized by the temperature increase of the permafrost above 18 m by at least 0.1°C and the PT declined by 2.46 m (Figure 4). However, the permafrost temperature changes under the shady side are more complicated. The temperature of the upper permafrost (defined the upper and lower parts with a depth of 7 m as before) is relatively stable and even the PT is rose due to less solar radiation. The lower permafrost of the shady side warmed but only slightly. The consumption of cold storage in the lower permafrost is the prerequisite for the thermal stability of the permafrost of the shady side, which means that this stability is not sustainable [48]. In the future, continued climate warming will eventually lead to the degradation of permafrost on the shady side, whether in upper or lower layers. The simulation results show that from 2020 to 2050, the depth of the PT will increase by more than 6 m under both the sunny and shady sides of the embankment, and the MAGT will increase by more than 0.2°C. For the embankment with unstable thermal regime, such as section K1068 + 750, strengthening measures should be taken in time, which can not only slow down the degradation of permafrost under the embankment but also adjust the asymmetry distribution of ground temperature on the sunny and shady sides. Studies have shown that crushed rock revetment, thermosyphons, and their composite forms, which can change the thermal convection between embankment and external environment, are the most commonly used and most effective strengthening measures along the QTR [21, 42, 49, 50]. The asymmetric setting of these measures can also help to change the uneven distribution of temperature on the sunny and shady sides of the

embankment, so as to avoid the formation of longitudinal cracks. Spraying materials with high albedo or putting the awning on the sunny slope of embankment can also slow down the warming of the permafrost on the sunny side by adjusting the radiation [46, 51].

5. Conclusion

In this study, the thermal regime of section K1068 + 750 was analysed by monitoring data, and the ground temperature change process of this section under climate warming was simulated by establishing a 2D heat transfer model. Based on the results, the degradation characteristics of permafrost under the embankment were studied. Furthermore, the unevenness of ground temperature caused by the sunny-shady slope effect was discussed. The following conclusions can be drawn:

(1) Since the operation of the QTR in 2006, the permafrost under section K1068 + 750 has been degrading. The combined effects of engineering activities and climate warming make the degradation rate faster than that of undisturbed sites. This indicates that the traditional embankment cannot maintain its thermal stability in such a badly unstable warm permafrost region.

(2) The asymmetry of solar radiation makes the degradation rate of permafrost on the sunny side and the shady side of the embankment different. On the sunny side, where radiation is stronger, the permafrost has been in a process of degradation since 2006, with the PT declining and the temperature increasing. On the shady side of the embankment, the thermal regime of permafrost is relatively stable in the first few years, but the simulation results show that the permafrost will eventually degenerate. For the section with insufficient stability, strengthening measures should be taken as soon as possible to slow down the warming of permafrost and adjust the ground temperature distribution on the sunny and shady sides.

Data Availability

The data used to support the findings of this study are available from the corresponding author upon request.

Conflicts of Interest

The authors declare that they have no conflicts of interest related to the publication of this manuscript.

References

[1] G. Cheng, "A roadbed cooling approach for the construction of qinghai-tibet railway," *Cold Regions Science and Technology*, vol. 42, no. 2, pp. 169–176, 2005.

[2] Q. B. Wu, G. D. Cheng, W. Ma, F. Niu, and Z. Z. Sun, "Technical approaches on permafrost thermal stability for qinghai-tibet railway," *Geomechanics and Geoengineering*, vol. 1, no. 2, pp. 119–127, 2006.

[3] G. D. Cheng, "Construction of qinghai-tibet railway with cooled roadbed," *China Railway Science*, vol. 24, no. 3, pp. 1–4, 2003.

[4] G. D. Cheng, "Interaction between Qinghai-Tibet Railway engineering and permafrost and environmental effects," *Bulletin of the Chinese Academy of Sciences*, vol. 17, no. 7, pp. 21–25, 2002.

[5] Y. H. Mu, W. Ma, Y. Z. Liu, and Z. Z. Sun, "Monitoring investigation on thermal stability of air-convection crushed-rock embankment," *Cold Regions Science and Technology*, vol. 32, no. 2-3, pp. 160–172, 2010.

[6] Q. Wu and F. Niu, "Permafrost changes and engineering stability in qinghai-xizang plateau," *Chinese Science Bulletin*, vol. 58, no. 10, pp. 1079–1094, 2013.

[7] W. Yu, W. Liu, L. Chen, X. Yi, F. Han, and D. Hu, "Evaluation of cooling effects of crushed rock under sand-filling and climate warming scenarios on the Tibet Plateau," *Applied Thermal Engineering*, vol. 92, pp. 130–136, 2016.

[8] W. Ma, G. Feng, Q. Wu, and J. Wu, "Analyses of temperature fields under the embankment with crushed-rock structures along the qinghai-tibet railway," *Cold Regions Science and Technology*, vol. 53, no. 3, pp. 259–270, 2008.

[9] W. Ma, Y. Mu, Q. Wu, Z. Sun, and Y. Liu, "Characteristics and mechanisms of embankment deformation along the qinghai-tibet railway in permafrost regions," *Cold Regions Science and Technology*, vol. 67, no. 3, pp. 178–186, 2011.

[10] Z. Z. Sun, W. Ma, S. J. Zhang, Z. Wen, and G. L. Wu, "Embankment stability of the qinghai–tibet railway in permafrost regions," *Journal of Cold Regions Engineering*, vol. 32, no. 1, pp. 1–7, 2018.

[11] Q. Wu, Y. Sheng, Q. Yu, J. Chen, and W. Ma, "Engineering in the rugged permafrost terrain on the roof of the world under a warming climate," *Permafrost and Periglacial Processes*, vol. 31, no. 3, pp. 417–428, 2020.

[12] H. Liu, F. Niu, and H. Guan, "An engineering evaluation index of thermal asymmetry in subgrade and its optimal design in cold regions," *Cold Regions Science and Technology*, vol. 137, pp. 1–6, 2017.

[13] Y. L. Chou, Y. Sheng, Y. W. Li et al., "Sunny-shady slope effect on the thermal and deformation stability of the highway embankment in warm permafrost regions," *Cold Regions Science and Technology*, vol. 63, no. 1-2, pp. 78–86, 2010.

[14] Y. Song, L. Jin, H. Peng, and H. Liu, "Development of thermal and deformation stability of qinghai-tibet highway under sunny-shady slope effect in southern tanglha region in recent decade," *Soils and Foundations*, vol. 60, no. 2, pp. 342–355, 2020.

[15] Y. Mu, W. Ma, Q. Wu, Z. Sun, Y. Liu, and G. Qu, "Thermal regime of conventional embankments along the qinghai-tibet railway in permafrost regions," *Cold Regions Science and Technology*, vol. 70, pp. 123–131, 2012.

[16] Y. H. Mu, W. Ma, F. J. Niu, Y. Z. Liu, R. Fortier, and Y. C. Mao, "Long-term thermal effects of air convection embankments in permafrost zones: case study of the qinghai–tibet railway, China," *Journal of Cold Regions Engineering*, vol. 32, no. 4, pp. 1–10, 2018.

[17] Z.-z. Sun, W. Ma, S.-j. Zhang, Y.-h. Mu, H.-b. Yun, and H.-l. Wang, "Characteristics of thawed interlayer and its effect on embankment settlement along the qinghai-tibet railway in permafrost regions," *Journal of Mountain Science*, vol. 15, no. 5, pp. 1090–1100, 2018.

[18] F. Niu, M. Liu, G. Cheng, Z. Lin, J. Luo, and G. Yin, "Long-term thermal regimes of the qinghai-tibet railway embankments in plateau permafrost regions," *Science China Earth Sciences*, vol. 58, no. 9, pp. 1669–1676, 2015.

[19] J. Luo, F. Niu, M. Liu, Z. Lin, and G. Yin, "Field experimental study on long-term cooling and deformation characteristics of crushed-rock revetment embankment at the qinghai-tibet railway," *Applied Thermal Engineering*, vol. 139, pp. 256–263, 2018.

[20] Q. Wu, H. Zhao, Z. Zhang, J. Chen, and Y. Liu, "Long-term role of cooling the underlying permafrost of the crushed rock structure embankment along the qinghai-xizang railway," *Permafrost and Periglacial Processes*, vol. 31, no. 1, pp. 172–183, 2019.

[21] Y. Hou, Q. Wu, J. Dong, J. Luo, M. Zhang, and Z. Ye, "Numerical simulation of efficient cooling by coupled RR and TCPT on railway embankments in permafrost regions," *Applied Thermal Engineering*, vol. 133, pp. 351–360, 2018.

[22] M. H. Liu, F. J. Niu, J. Luo, G. A. Yin, and L. Zhang, "Performance, applicability, and optimization of a new slope cooling and protection structure for road embankment over warm permafrost," *International Journal of Heat and Mass Transfer*, vol. 162, Article ID 120388, 2020.

[23] B. W. Tai, Q. B. Wu, Z. Q. Zhang, and X. M. Xu, "Study on thermal performance of novel asymmetric crushed-rock-based embankment on the qinghai-tibet railway in permafrost region," *International Journal of Thermal Sciences*, vol. 152, Article ID 106333, 2020.

[24] H. L. Wu, J. Liu, and X. Zhang, "Feasibility study on use of cellular concrete for air convection embankment on permafrost foundations in fairbanks, alaska," *Transportation Geotechnics*, vol. 22, Article ID 100317, 2020.

[25] S. Y. Li, Y. M. Lai, M. Y. Zhang, and Y. H. Dong, "Study on long-term stability of qinghai–tibet railway embankment," *Cold Regions Science and Technology*, vol. 57, no. 2-3, pp. 139–147, 2009.

[26] L. Chen, W. Yu, X. Yi, D. Hu, and W. Liu, "Numerical simulation of heat transfer of the crushed-rock interlayer embankment of qinghai-tibet railway affected by aeolian sand clogging and climate change," *Cold Regions Science and Technology*, vol. 155, pp. 1–10, 2018.

[27] C. X. Tang, Z. Y. Zhu, F. Luo, Z. H. He, Z. Y. Zou, and X. H. Guo, "Deformation behaviour and influence mechanism of thaw consolidation of embankments on the qinghai-tibet railway in permafrost regions," *Transportation Geotechnics*, vol. 28, Article ID 100513, 2021.

[28] X. Hou, J. Chen, H. Jin, P. Rui, J. Zhao, and Q. Mei, "Thermal characteristics of cast-in-place pile foundations in warm permafrost at beiluhe on interior qinghai-tibet plateau: field observations and numerical simulations," *Soils and Foundations*, vol. 60, no. 1, pp. 90–102, 2020.

[29] G. S. Taylor and J. N. Luthin, "A model for coupled heat and moisture transfer during soil freezing," *Canadian Geotechnical Journal*, vol. 15, no. 4, pp. 548–555, 1978.

[30] W. D. An, *Interaction Among Temperature, Moisture and Stress Fields in Frozen Soil*, Lanzhou University Press, Lanzhou, China, 1990.

[31] Y. Lai, W. Pei, and W. Yu, "Calculation theories and analysis methods of thermodynamic stability of embankment engineering in cold regions," *Chinese Science Bulletin*, vol. 59, no. 3, pp. 261–272, 2014.

[32] M. Zhang, X. Zhang, S. Li et al., "Evaluating the cooling performance of crushed-rock interlayer embankments with unperforated and perforated ventilation ducts in permafrost regions," *Energy*, vol. 93, pp. 874–881, 2015.

[33] X. Z. Xu, J. C. Wang, and L. X. Zhang, *Physics of Frozen Soil*, Science Press, Beijing, China, 2001.

[34] Y. M. Lai, M. Y. Zhang, and S. Y. Li, *Theory and Application of Cold Regions Engineering*, Science Press, Beijing, China, 2009.

[35] D. H. Qin, *The Comprehensive Evaluating Report on the Environment Evolvement in West China*, Science Press, Beijing, China, 2002.

[36] L. N. Zhu, "Study of the adherent layer on different types of ground in permafrost regions on the qinghai-xizang plateau," *Journal of Glaciology and Geocryology*, vol. 10, no. 1, pp. 35–39, 1988.

[37] Y. Lai, L. X. Zhang, S. J. Zhang, and L. Mi, "Cooling effect of ripped-stone embankments on qing-tibet railway under climatic warming," *Chinese Science Bulletin*, vol. 48, no. 6, pp. 598–604, 2003.

[38] C. J. Tong and Q. B. Wu, "The effect of climate warming on the qinghai-tibet highway, China," *Cold Regions Science and Technology*, vol. 24, no. 1, pp. 101–106, 1996.

[39] Q. B. Wu, B. Shi, and H. Y. Fang, "Engineering geological characteristics and processes of permafrost along the qinghai–xizang (tibet) highway," *Engineering Geology*, vol. 68, no. 3-4, pp. 387–396, 2003.

[40] H.-j. Jin, Q.-h. Yu, S.-l. Wang, and L.-z. Lü, "Changes in permafrost environments along the qinghai-tibet engineering corridor induced by anthropogenic activities and climate warming," *Cold Regions Science and Technology*, vol. 53, no. 3, pp. 317–333, 2008.

[41] W. Ma, Y. H. Mu, J. M. Zhang, W. B. Yu, Z. W. Zhou, and T. Chen, "Lateral thermal influences of roadway and railway embankments in permafrost zones along the qinghai-tibet engineering corridor," *Transportation Geotechnics*, vol. 21, Article ID 100285, 2019.

[42] Q.-H. Mei, J. Chen, J.-C. Wang et al., "Strengthening effect of crushed rock revetment and thermosyphons in a traditional embankment in permafrost regions under warming climate," *Advances in Climate Change Research*, vol. 12, no. 1, pp. 66–75, 2021.

[43] M. Zhang, Y. Lai, Z. Gao, and W. Yu, "Influence of boundary conditions on the cooling effect of crushed-rock embankment in permafrost regions of qinghai-tibetan plateau," *Cold Regions Science and Technology*, vol. 44, no. 3, pp. 225–239, 2006.

[44] Z. Kun, D. Li, N. Fujun, and M. Yanhu, "Cooling effects study on ventilated embankments under the influence of the temperature differences between the sunny slopes and the shady slopes," *Cold Regions Science and Technology*, vol. 65, no. 2, pp. 226–233, 2011.

[45] M. Zhang, W. Pei, S. Li, J. Lu, and L. Jin, "Experimental and numerical analyses of the thermo-mechanical stability of an embankment with shady and sunny slopes in a permafrost region," *Applied Thermal Engineering*, vol. 127, pp. 1478–1487, 2017.

[46] J. Chenji, Z. Y. Huzeyong, S. Doushun, and Z. Y. Qianzeyu, "Yin-yang slope problem along qinghai-tibetan lines and its radiation mechanism," *Cold Regions Science and Technology*, vol. 44, no. 3, pp. 217–224, 2006.

[47] B. Tai, J. Liu, Z. Yue, J. Liu, Y. Tian, and T. Wang, "Effect of sunny-shady slopes and strike on thermal regime of subgrade along a high-speed railway in cold regions, China," *Engineering Geology*, vol. 232, pp. 182–191, 2018.

[48] J. Liu, B. Tai, and J. Fang, "Ground temperature and deformation analysis for an expressway embankment in warm

permafrost regions of the tibet plateau," *Permafrost and Periglacial Processes*, vol. 30, no. 3, pp. 208–221, 2019.

[49] W. Ma, Z. Wen, Y. Sheng, Q. Wu, D. Wang, and W. Feng, "Remedying embankment thaw settlement in a warm permafrost region with thermosyphons and crushed rock revetment," *Canadian Geotechnical Journal*, vol. 49, no. 9, pp. 1005–1014, 2012.

[50] Y. D. Hou, Q. B. Wu, Y. Z. Liu, Z. Q. Zhang, and S. R. Gao, "The thermal effect of strengthening measures in an insulated embankment in a permafrost region," *Cold Regions Science and Technology*, vol. 116, pp. 49–55, 2015.

[51] W. J. Feng, W. Ma, L. X. Zhang, and Z. J. Wu, "Application of awning to roadway engineering in permafrost regions," *Chinese Journal of Geotechnical Engineering*, vol. 25, no. 5, pp. 567–570, 2003.